A Simple Model for Correcting Sodar and Lidar Errors in Complex Terrain

STUART BRADLEY

Physics Department, University of Auckland, Auckland, New Zealand

(Manuscript received 23 May 2012, in final form 27 September 2012)

ABSTRACT

Ground-based sensing of wind profiles by sodars and lidars is becoming the standard for wind energy and other applications. However, there remain difficulties in complex terrain since the instruments sense wind components in spatially separated volumes, and systematic spatial variations of the wind components can lead to systematic bias in wind estimation. The errors are typically less than 6%, so corrections do not need to be very sophisticated.

Analytic potential flow models are developed for the flow over a bell-shaped hill and over an escarpment. These models are then used to find the radial Doppler shift from sampling volumes in typical sodar and lidar beam geometries, thereby allowing spatial variation bias to be removed. Since the models are straightforward, bias removal is readily achieved, and also lends itself to an understanding of the significant parameters affecting wind errors.

The bell model is tested against field data from sodars and lidars in both moderately complex and in very complex terrain. It is found that corrected winds are to within approximately 1% of those measured by mast instruments. Much more complex models do not correct wind errors better than these simple models.

1. Introduction

Lidars and sodars measure the Doppler shift due to the radial component of wind along off-vertical beam directions. Measurements from three or more beam directions are used to build up the three components of the wind vector at each height. The assumption in this method is that the same wind is present in each of the volumes sampled by the various beam directions (Bradley 2007).

Very good wind estimates are obtained by both lidars and sodars if this assumption is true. Comparisons with mast-mounted instruments, on flat terrain, and with steady flow, have shown correlations with $R^2 > 0.985$ for both lidars and sodars (UpWind 2011).

When wind flow is not horizontally homogeneous (in complex terrain), the radial wind equations contain different wind components. For example, a three-beam system sampling three separate volumes at a particular height will have u_1, u_2, and u_3 for the easterly wind component instead of just u, and nine wind components in total, instead of just three (Bingol et al. 2009). Behrens et al. (2012) and Bradley et al. (2012) have shown that measurements using conventional lidar or sodar technology show up to 8% errors in wind speed estimates in complex terrain, when compared with mast-mounted instruments. Such errors are unacceptably large for wind resource estimation or for turbine power monitoring. In this situation, the mast instruments measure in a single volume at a particular height, and so do not show errors due to horizontal variability of the wind.

Bingol et al. (2009) use a relatively complex model to correct the errors arising from use of a lidar in complex terrain. Here we consider a simple 2D hill model with only 2D flow. This is not as restrictive as might first be thought. Tests on real hills show the 2D approximation, applied to a cross section of the topography in the direction of flow, agrees with full 3D models (see section 5). The motivation for the present study is that analytic results can be obtained that allow the systematic spatial variations of wind vector components to be easily characterized through their functional dependencies on factors such as on hill height and hill width. Into this flow field we can embed typical sodar and lidar beam geometries and analytically determine the dependence of wind errors on beam tilt angle, beam orientation with respect to the ridge, and instrument distance upstream or downstream of the ridge.

Corresponding author address: Stuart Bradley, Physics Department, University of Auckland, Private Bag 92019, Auckland, New Zealand.
E-mail: s.bradley@auckland.ac.nz

DOI: 10.1175/JTECH-D-12-00106.1

2. Flow over a bell-shaped hill

The basis for our flow model is to use analytic solutions for the streamlines of potential flow over simple obstacles, for the case where the flow a long way upstream is uniform. By definition, a streamline is a line across which there is no flow. For 2D flow a streamline defines a surface through which there is no flow, and flow over this surface is indistinguishable from flow over the same *solid* surface. There are two major advantages to our approach. First, the flow is analytic, and so fast to compute and also readily analyzed to identify the important scaling parameters. Second, at infinite distance from the generating obstacle, the flow will be undisturbed. This means that the streamlines will vary smoothly in slope as their upstream distance from the centerline varies. It is therefore possible to choose a streamline which models more or less complex hill slopes.

We first consider the streamlines generated by potential flow over a cylinder, (Bradley 2008). Consider uniform horizontal flow of speed U in the $+x$ direction incident on a cylinder centered on the origin in a rectangular Cartesian coordinate system (x, y, η). We use η because later we want to identify z with the height above the streamline we choose to define the solid ground surface. The potential flow solution gives the following streamfunction:

$$\psi = U\eta\left(1 - \frac{a^2}{x^2 + \eta^2}\right), \tag{1}$$

where a is the radius of the cylinder. Streamlines are defined by

$$\eta_0 = \eta\left(1 - \frac{a^2}{x^2 + \eta^2}\right). \tag{2}$$

These streamlines have a bell shape with maximum elevation H above η_0 occurring at $x = 0$, with

$$H = \frac{1}{2}\left(\sqrt{\eta_0^2 + 4a^2} - \eta_0\right). \tag{3}$$

The geometry in shown in Fig. 1. Any such streamline, defined by a and η_0, can be considered to be a solid surface, thereby defining a useful set of bell-shaped hill profiles having larger width-to-height ratios as η_0 increases. Plotting such streamlines for moderately complex terrain comprising rolling hills shows that the hill height h above the surrounding terrain satisfies $h = \eta - \eta_0 \ll \eta_0$.

The hill half-width L at half height is

$$L = \eta_0\left[1 + \frac{H}{\eta_0} + \frac{3}{4}\left(\frac{H}{\eta_0}\right)^2\right]^{1/2} \approx \eta_0. \tag{4}$$

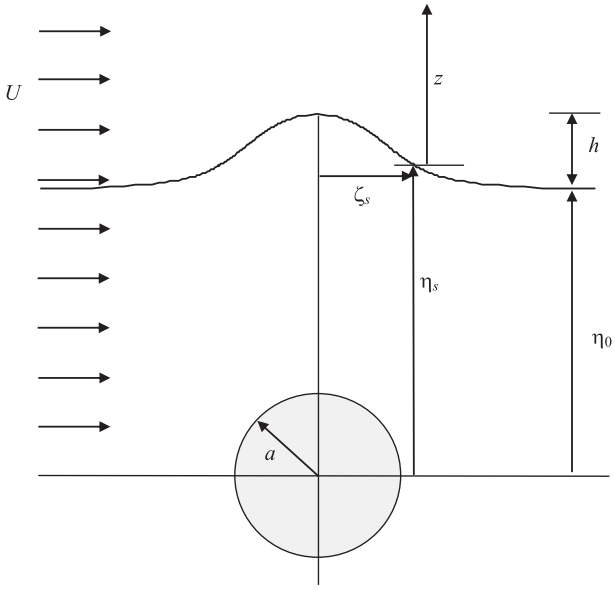

FIG. 1. Potential flow over a cylinder of radius a gives streamlines defined by their lateral separation at infinity, η_0. The surface of a hill of height h is defined by choosing a streamline of the required curvature, and the wind speed components can then be found at a height z above the surface coordinates (ζ_s, η_s).

Combining (3) and (4) gives

$$\eta_0 = \left(L^2 + \frac{H^2}{4}\right)^{1/2} - H,$$
$$a^2 = HL\left[1 + \left(\frac{H}{2L}\right)^2\right]^{1/2} \approx HL. \tag{5}$$

Equation (2) can be rewritten in terms of the hill height above the terrain in the following form:

$$h = \eta - \eta_0 = (\eta_0 + h)\frac{a^2}{x^2 + (\eta_0 + h)^2} \approx \frac{\eta_0 a^2}{x^2 + \eta_0^2}. \tag{6}$$

Making use of the approximations in (4) and (5),

$$\frac{h}{H} = \frac{1}{\left(\frac{x}{L}\right)^2 + 1}. \tag{7}$$

This is a version of the ''Witch of Agnesi'' and defines a simple bell-shaped hill profile. The maximum hill slope, which can be used to define the complexity, is now readily found to be $[(9/8)3^{-1/2}](H/L)$ at $x = \pm L/3^{1/2}$. For $H/L = 0.1$, the approximation in (7), is within $0.01H$ of the potential flow height given by (2), over $x = -L$ to $+L$.

Now consider the case where measurements are made at a height z above the hill surface, so $\eta = \eta_0 + h + z$. The flow velocity components u and w are

$$\frac{u}{U} = \frac{1}{U}\frac{\partial\psi}{\partial\eta} = 1 + a^2\frac{\eta^2 - x^2}{(\eta^2 + x^2)^2}$$
$$\approx 1 + \frac{H}{L}\frac{(1 + \{h+z\}/L)^2 - (x/L)^2}{[(1 + \{h+z\}/L)^2 + (x/L)^2]^2}$$
$$\frac{w}{U} = -\frac{1}{U}\frac{\partial\psi}{\partial x} = a^2\frac{2x\eta}{(\eta^2 + x^2)^2}$$
$$\approx 2\frac{H}{L}\frac{1 + \{h+z\}/L}{[(1 + \{h+z\}/L)^2 + (x/L)^2]^2}\frac{x}{L}. \quad (8)$$

When $x = 0$, the speed up is a maximum at

$$\frac{u_{\max}}{U} = 1 + \frac{H}{L}\frac{1}{(1 + \{H+z\}/L)^2}. \quad (9)$$

Equations (7) and (8) can be combined to give expressions for u and w as rational polynomials in x. Frequently the interest is near the hill ridge, where $x \ll L$, and then (8) may be approximated by

$$\frac{u}{U} \approx 1 + \frac{H}{L}\left[1 - 3\left(\frac{x}{L}\right)^2 - 2\frac{H}{L}\frac{z}{H}\right]$$
$$\frac{w}{U} \approx 2\frac{H}{L}\frac{x}{L}\left[1 - 2\left(\frac{x}{L}\right)^2 - 3\frac{H}{L}\frac{z}{H}\right]. \quad (10)$$

Over the range $-0.4 < x/L < 0.4$, the approximate scaled horizontal wind speed components u and w from (10) agree with the exact potential flow solutions to within 10%.

3. Inserting a sodar or lidar into the flow

Figure 2 shows the geometry for a sodar or lidar situation at a distance x_s from the hill peak. For simplicity we will consider a three-beam sodar with beam 1 having zenith angle θ and azimuth angle ϕ, beam 2 having zenith angle θ and azimuth angle $\phi + 90°$, and beam 3 being vertical. This is the configuration of an ASC4000 sodar, for example. At each height z above the surface, measurements m_1, m_2, and m_3 are made on each beam of the radial Doppler shift, resulting in three equations which, without any correction for wind shear, have the following form:

$$m_1 = u(x_s, z)\cos\varphi\sin\theta + v(x_s, z)\sin\varphi\sin\theta + w(x_s, z)\cos\theta$$
$$m_2 = -u(x_s, z)\sin\varphi\sin\theta + v(x_s, z)\cos\varphi\sin\theta + w(x_s, z)\cos\theta$$
$$m_3 = w(x_s, z). \quad (11)$$

These are solved to give the following:

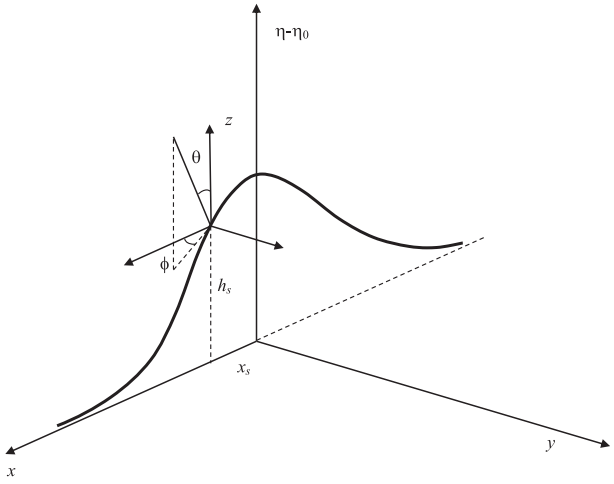

FIG. 2. Geometry of a sodar or lidar at (x_s, h_s) on the hill surface. One beam is shown, with zenith angle θ and azimuth angle ϕ.

$$u(x_s, z) = \left(\frac{m_1 - m_3\cos\theta}{\sin\theta}\right)\cos\varphi + \left(\frac{m_2 - m_3\cos\theta}{\sin\theta}\right)\sin\varphi$$
$$v(x_s, z) = \left(\frac{m_1 - m_3\cos\theta}{\sin\theta}\right)\sin\varphi + \left(\frac{m_2 - m_3\cos\theta}{\sin\theta}\right)\cos\varphi$$
$$w(x_s, z) = m_3. \quad (12)$$

However, the sampling volumes from beams 1 and 2 are not directly above the instrument, so the measurement equations should be, for the case $v = 0$:

$$m_1 = u_1\cos\phi\sin\theta + w_1\cos\theta$$
$$m_2 = -u_2\sin\phi\sin\theta + w_2\cos\theta$$
$$m_3 = w_3, \quad (13a)$$

where

$$u_1 = u(x_s + z\tan\theta\cos\phi, z)$$
$$w_1 = w(x_s + z\tan\theta\cos\phi, z)$$
$$u_2 = u(x_s - z\tan\theta\sin\phi, z)$$
$$w_2 = w(x_s - z\tan\theta\sin\phi, z)$$
$$w_3 = w(x_s, z). \quad (13b)$$

The estimated wind vector components, without any correction for wind shear, are as follows:

$$\hat{u} = u_1\cos^2\varphi + u_2\sin^2\varphi + \frac{w_1 - w_3}{\tan\theta}\cos\varphi - \frac{w_2 - w_3}{\tan\theta}\sin\varphi$$
$$\hat{v} = (u_1 - u_2)\sin\varphi\cos\varphi + \frac{w_1 - w_3}{\tan\theta}\sin\varphi + \frac{w_2 - w_3}{\tan\theta}\cos\varphi$$
$$\hat{w} = w_3. \quad (14)$$

The components u_1, w_1, u_2, w_2, and w_3 can be approximated using (10). The errors $\Delta u = \hat{u} - u(x_s, z)$ and

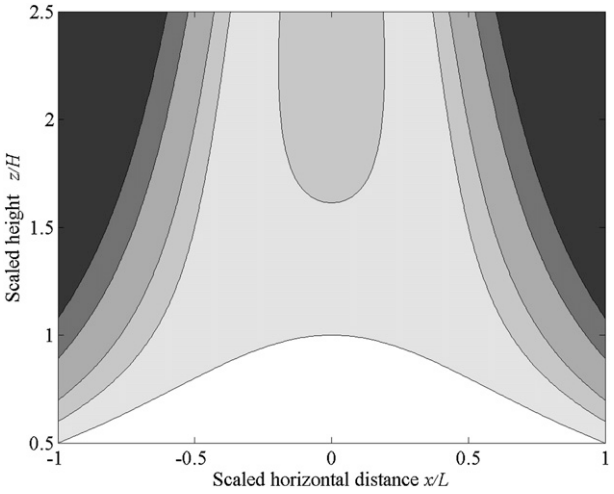

FIG. 3. Contours of percentage error in wind speed for the case $H/L = 0.1$. The lower white portion is the hill, and the progressively darker areas have borders of 1%, 2%, 4%, and 6% error.

$\Delta v = \hat{v} - v(x_s, z)$ can then be found explicitly in terms of hill parameters. For other instrument beam geometries a similar procedure can be followed, but the three errors will differ. For example, the AQSystem AQ500 sodar has three inclined beams and also produces a Δw error.

For simplicity, consider the case $\phi = 0$. Then

$$\frac{\Delta u}{U} \approx 2\left(\frac{H}{L}\right)^2 \frac{z}{H}\left[1 - 6\left(\frac{x}{L}\right)^2 - 3\frac{H}{L}\frac{z}{H}\right] \qquad (15)$$

and $\Delta v = \Delta w = 0$. The wind error is zero at the ground, since here there is no separation between sampling volumes. At the hill peak ($x = 0$), the estimated wind is lower than the wind above the peak, because the sampling volume for beam 1 is away from the wind maximum, which is above the hill peak. There is a maximum absolute error at $z = L/6$, which is generally much higher than will be observed on a sodar or lidar. As an example of the magnitude of error that might be expected, for a hill having $H = 100$ m and $L = 1$ km, and at a height of $z = 200$ m, the wind speed error will be 4%. Figure 3 shows error contours for $H/L = 0.1$.

4. Flow over a Schwarz–Christoffel step

The above treatment gives an analytic model for a symmetric hill. It is also possible to conduct a similar treatment for the potential flow over an escarpment. We use the Schwarz–Christoffel conformal mapping of a line into a step of height H. Here

$$\zeta = \frac{\pi}{HU}(\phi + i\psi), \qquad (16)$$

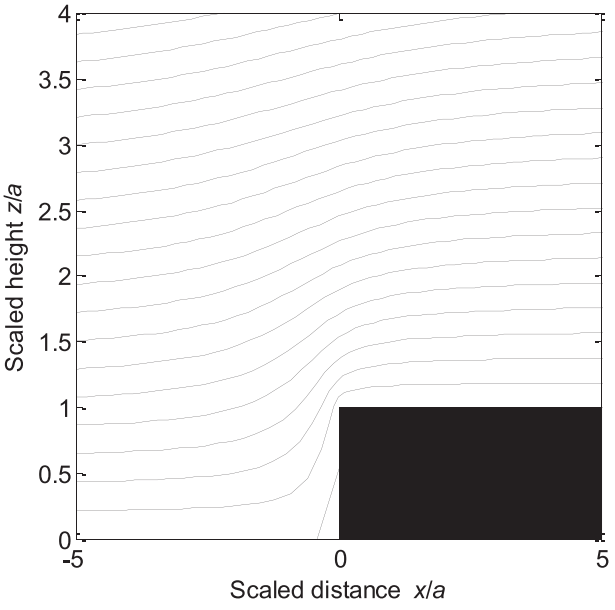

FIG. 4. Streamlines based on a Scharwz–Christofell step conformal mapping.

where φ is the velocity potential and ψ is the streamfunction. Then

$$x + i\eta = \frac{H}{\pi}\left[\sqrt{\zeta^2 - 1} + \ln\left(\zeta + \sqrt{\zeta^2 - 1}\right)\right] \qquad (17)$$

gives the coordinates (x, η) of streamlines for constant ψ values (see Fig. 4). Examination of the asymptotic behavior of (17) leads to the approximations

$$x = \frac{\phi}{U} \quad \eta = \frac{\psi}{U} + H\left(\frac{1}{2} - \frac{1}{\pi}\tan^{-1}\frac{Ux}{\psi}\right). \qquad (18)$$

Choosing a streamline defined by $\psi = \psi_0$ as the hill profile, gives hill shape

$$h = H\left(\frac{1}{2} - \frac{1}{\pi}\tan^{-1}\frac{Ux}{\psi_0}\right). \qquad (19)$$

At $x = 0$, the slope of the hill is, from (18) and (19), $-H/(\pi L)$ where $L = \psi_0/U$. Near the escarpment, and for moderate slopes, ψ_0 is large and ϕ is small, so

$$\frac{h}{H} \approx \frac{1}{2} - \frac{1}{\pi}\frac{x/L}{1 + (x/L)^2}. \qquad (20)$$

Examination of the streamlines in Fig. 4, particularly the lowermost streamlines, shows that there is a low velocity region upstream of the hill and an intensification of the wind speed above the step. Above the step change the wind speed is higher, but much of this is due to an

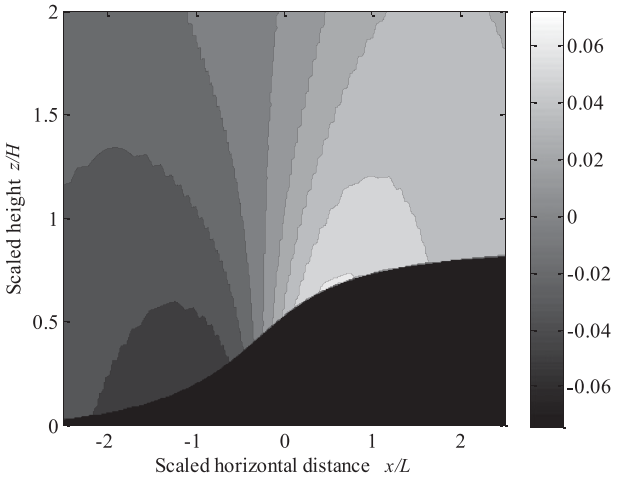

FIG. 5. Fractional error in wind speed for flow over an escarpment having a maximum slope of 0.1, with the error scale given at the right.

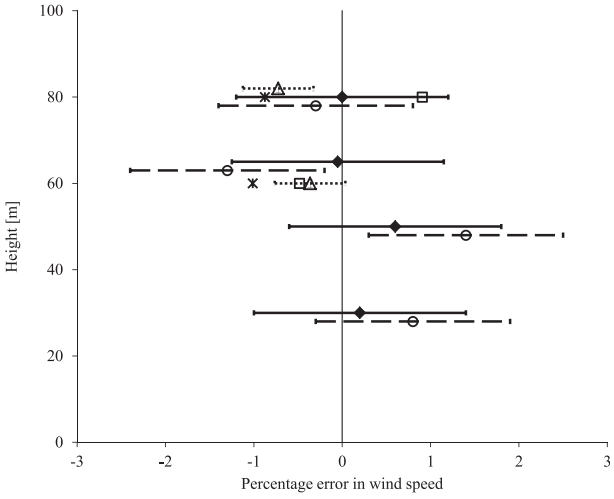

FIG. 6. Percentage error in wind estimation following correction using the bell hill model at a moderately complex site (Myres Hill) and a very complex site (Turitea). Measurements are at Myres Hill with a sodar (solid diamond and heavy error bars) and a lidar (open circles and dashed error bars), and at Turitea with a sodar (open triangle and dotted error bars). Measurement heights have been offset so that the error bars can be clearly seen. Also shown are the OpenFOAM (asterisk) and WindSim (square) model results.

increase in vertical velocity component. The error in estimated wind speed is found in a similar manner to that of the bell hill. Figure 5 shows the fractional error versus height above a three-beam sodar placed at any position on the hill surface, with beam 1 facing upstream. Near the base of the escarpment beam 1 samples a volume closer to the foot of the hill and underestimates the wind above the sodar. The converse is true if the sodar is placed above the hill half-height. Substantial errors extend both upstream and downstream of the point of maximum slope.

5. Comparison between the model and measurements

Measurements have been conducted at two complex terrain sites where there were well-instrumented masts (see Emeis 2010). The first was at the at the Myres Hill wind turbine test site in Scotland (Bradley et al. 2012), equipped with an 80-m meteorological mast, a ZephIR lidar, and AQ500 sodar. The site is an escarpment type with a hill height of about 50 m and a maximum slope of around 0.2. However, we modeled this hill using a double-bell shape because it was not flat at the top of the hill. Since the bell model is linear, it is relatively straightforward to add two bells. The result was that we modeled the whole relevant hill profile to an rms height variation of 2 m. The second site was at Turitea in the North Island of New Zealand (Behrens et al. 2012). This was a much more complex site, with a ridge running approximately perpendicular to the flow. Winds estimated by instrumentation on an 80-m mast were compared with those from a Metek PCS2000 sodar. In this case, because of concerns about the complexity, two other much more detailed flow models, WindSim (www.windsim.com) and OpenFOAM (www.openfoam.com), were also used to estimate wind shear corrections for the sodar. In Fig. 6 we show the residual percentage wind speed errors, treating the mast data as ''correct,'' after correcting the data from both sites using the simple potential flow models. Also shown are the predictions from OpenFOAM and WindSim, corrected using the potential flow model. While there are some fluctuations with height and between instruments, the corrections based on the simple potential flow theory reduce measurement errors to generally less than 1%, as compared with the original errors of typically 6%. Error bars show standard error divided by mean wind speed, as a percentage. The quality of the corrections is similar for the moderate and the more complex sites. It is interesting that a full computational fluid dynamics (CFD) model such as OpenFOAM does not perform corrections as well as the potential flow model (see Behrens et al. 2012).

6. Conclusions

We have developed analytic potential flow models for the flow over a bell-shaped hill and over an escarpment. These models are then used to find the radial Doppler shift from sampling volumes in typical sodar and lidar beam geometries. In general in complex terrain sites, these sampling volumes are not directly above the instrument and the spatial variation of the wind

causes bias in the wind estimations. This bias can be corrected by combining the instrument geometry with the predicted flow field. Since the model is straightforward, bias can readily be corrected, and the model also lends itself to an understanding of the significant parameters affecting wind errors.

For the bell hill model we have also approximated the hill shape and the flow to simple quadratic forms, which are shown to closely match the exact potential flow solutions. This type of approximation may also be possible for the escarpment model, although we have not attempted that here.

The bell model is tested against field data from sodars and lidars in both moderately complex and in very complex terrain. It is found that corrected winds are to within about 1% of those measured by mast instruments. It is also found that much more complex computational fluid dynamics models do not correct wind errors better than our simple models. This is probably because the remaining errors are due to other causes, and the more complicated models are adding further uncertainty because of the need for more boundary conditions, which may not be well known. This is a significant result, because corrections for terrain errors are increasingly required in wind resource assessments, and operating complex models can more readily give incorrect outputs since selection of input parameters requires specialized skill. It is perhaps surprising that the potential flow corrections are successful, given that surface roughness is ignored. However, the terrain errors are zero at the surface because the sampling volumes are not separated there, so surface effects do not contribute strongly.

REFERENCES

Behrens, P., J. O'Sullivan, R. Archer, and S. Bradley, 2012: Underestimation of mono-static sodar measurements in complex terrain. *Bound.-Layer Meteor.,* **143,** 97–106.

Bingol, F., J. Mann, and D. Foussekis, 2009: Conically scanning lidar error in complex terrain. *Meteor. Z.,* **18,** 189–195.

Bradley, S. G., 2007: *Atmospheric Acoustic Remote Sensing.* CRC Press/Taylor and Francis Group, 328 pp.

——, 2008: Wind speed errors for LIDARs and SODARs in complex terrain. *IOP Conf. Ser.: Earth Environ. Sci.,* **1,** 1–7, 012061, doi:10.1088/1755-1315/1/1/012061.

——, Y. Perrott, and A. Oldroyd, 2012: Corrections for wind-speed errors 411 from sodar and lidar in complex terrain. *Bound.-Layer Meteor.,* **143,** 37–48.

Emeis, S., 2010: *Measurement Methods in Atmospheric Sciences: In Situ and Remote.* Borntraeger Science Publishers, 257 pp.

UpWind, cited 2011: UpWind EU project. [Available online at http://www.upwind.eu.]